Article

Journal of the Brazilian Chemical Society

https://dx.doi.org/10.21577/0103-5053.20240169

*J. Braz. Chem. Soc.* **2025**, *36*, 3, e-20240169, 1-15


# Theoretical and Experimental Study of the Process for Obtaining PAni(DBSA) - Part I: Formation of the Anilinium-DBS Salt

***Eudes R. S. Silva,[a] José D. dos Santos[a] and Olacir A. Araújo*** *,[a]

[a]*Laboratório de Química de Materiais e Modelagem Molecular (QMMOL), Universidade Estadual de Goiás, 75132-903 Anápolis-GO, Brazil*

The first step in the synthesis of polyaniline doped with dodecylbenzene sulfonic acid is the synthesis of the anilinium dodecylbenzene sulfonate salt obtained through the reaction between aniline and dodecylbenzene sulfonic acid in aqueous medium. In this work, theoretical models were developed to simulate the formation mechanism of this salt in an aqueous medium. Changes in energy, frontier orbitals, gap energy, charge distribution and thermodynamic parameters were calculated. These theoretical results were correlated with the experimental data from the synthesis of the salt and from infrared spectroscopy. Theoretical models suggested that the solubilization of dodecylbenzene sulfonic acid and aniline in water are energetically and thermodynamically favorable processes. Interactions between the frontier orbitals indicated the formation of water-insoluble anilinium dodecylbenzene sulfonate salt. These molecular modeling results agree with experimental data indicating that the theoretical method used was efficient in simulating the reaction system.

**Keywords:** conducting polymers, frontier orbitals, molecular modeling, aniline

## Introduction

Polyaniline (PAni) is an intrinsically conductive polymer (ICP) that stands out for its potential technological applications stemming from its electrical properties. Characteristics such as easy synthesis, low cost, easy acquisition of the monomer and chemical stability in ambient conditions, when compared to other ICP, make its study more attractive.[1-7]

PAni has been used in several processes, such as work on the development of Schottky diodes,[3] chemical sensors,[8] pressure,[9] and glucose monitoring in humans,[10] humidity sensors,[11] electromechanical devices,[12] surface coating,[13-15] anticorrosive additive in paints,[16] photodegradation,[17,18] cathode in batteries,[19-21] superconductors,[22] electrically responsive membranes,[23] adsorptions,[24,25] oxygen reduction reaction catalysts,[26] microsupercapacitors,[27] increased conductivity in electrodes,[28] among others.

PAni is obtained by the polymerization of aniline, through the following methods: enzymatic,[6] electrochemical,[19] ultrasonic irradiation,[29] photochemical, metathesis, by inclusion, solid-state, plasmatic, among others or by chemical synthesis in an acid medium using an oxidizing agent,[24] which is the most widely used when large-scale production is required.

Polyaniline can be obtained in three main forms: leucoemeraldine base (LB, the totally reduced form), emeraldine base (EB, partially oxidized form) and pernigraniline base (PB, fully oxidized form).[30-32] None of these have significant electrically conductive properties, however, from the protonation of EB, a process also known as doping,[6] it is possible to obtain the form that demonstrates expressive electrically conductive characteristics, in the order of 10 S $cm^{-1}$, known as emeraldine salt (ES).[7,33] The protonation or doping of PAni can be obtained during the synthesis, if carried out in an acid medium, or later, by exposing the emeraldine base to the presence of a protonic acid.[34]

Dodecylbenzene sulfonic acid (DBSA), as well as other long-chain alkyl-type sulfonic acids such as camphorsulfonic acid, β-naphthalene sulfonic acid, *p*-toluene sulfonic acid,[35] have stood out among the organic acids used in the synthesis and doping of PAni both for the resulting good solubility in common solvents,[5] good processability and electrical conductivity,[21,30] and for the stability and maintenance of the mechanical properties of conventional polymers, and acts simultaneously in the

*e-mail: olacir.araujo@ueg.br
Editor handled this article: Paula Homem-de-Mello (Associate)

synthesis process, as a dopant and as a surfactant.[36]

Methods used in quantum mechanics can contribute to the development of theoretical studies of properties, interactions, formation and the breaking of bonds, among other characteristics of a microscopic system, helping to understand the mechanisms and, consequently, reducing the time spent searching for this information in the laboratory.[37]

There is a body of work in which quantum mechanical methods were used to study the structure of PAni dating back to 1986, when the semi-empirical MNDO (modified neglect of diatomic overlap) method was already used to calculate some properties of PAni, aniline and their dimers and trimers, such as geometries, redox potentials and band gaps[38] and, there are also reports of other theoretical works on PAni and its precursors with results that reproduced some experimental data from the time. Since then, several works have been completed, investigating: (*i*) the hydrogen bonds formed between PAni and water;[33] (*ii*) the changes caused in the frontier orbitals in aniline tetramers due to the presence of ZnO;[39] (*iii*) increase in stability related to the growth of the PAni polymer chain;[40] (*iv*) interaction of PAni@HTS (polyaniline@hematite-titaniferous sand) with orthophosphates;[41] (*v*) the effect of including side groups in PAni;[42] (*vi*) interaction of PAni/ZnO with methylene blue;[43] (*vii*) interaction between the aniline structure 18 and the structure of aniline with a silver surface;[44] (*viii*) investigation of electrical conductivity in emeraldine salt;[45] (*ix*) study of PAni anchoring in SARS-Cov-2 (severe acute respiratory syndrome coronavirus 2),[46] among others.

## Experimental

The methodology was divided into two parts: experimental methods and molecular modeling. The organization of the work was designed so that the results obtained in the experimental methods would lead to molecular modeling.

### Experimental method

#### Synthesis of anilinium-DBS (anilinium-dodecylbenzene sulfonate) salt

The amount of 9.33 g (0.0286 mol) of DBSA (purchased from Chemco, Hortolândia, Brazil) were dissolved in 50 mL of water in a beaker, then 2.6 mL (0.0285 mol) of aniline (purchased from Neon, Suzano, Brazil) were added, forming a gelatinous white precipitate. This salt was filtered and washed with 1 L of ethanol (purchased from Labsynth, Diadema, Brazil) solution in electrodeionized water (2:3 v/v) (Gehaka Electrodeionizer, São Paulo, Brazil) to eliminate the maximum interference of residual reagents and by-products in the characterization of the salt, and dried in an oven Ethik 420 (Vargem Grande Paulista, Brazil) for 6 h at 90 °C.

#### Vibrational absorption spectroscopy in the mid-infrared region

Vibrational spectra were obtained in the infrared region (Fourier transform infrared (FTIR) spectroscopy) of aniline, DBSA and anilinium-DBS salt. The samples were dispersed in KBr and pressed into pellets. The spectra were recorded in the range of 4000-400 $cm^{-1}$ in a Spectrum Frontier FTIR MID-NIR PerkinElmer spectrometer (Waltham, USA), at the Center for Analysis, Innovation and Technology in Natural and Applied Sciences at Universidade Estadual de Goiás/CAITEC.

### Molecular modeling

In the simulation of the structures and interactions, semi-empirical methods were used and the first optimization of the geometry of the structures was carried out in MOPAC (Molecular Orbital PACkage) software.[47] Optimization calculations for chemical structures, interactions and other properties were performed using the Gaussian software, versions 03[48] and 09.[49] The parameters for choosing the software included the possibility of using it within the operational capabilities of the available computers, cost reduction (free software) and, in the case of Gaussian for availability, quality of results and popularization of its use.

Molecular modeling was performed according to the steps presented in Figure 1. The geometries of the following individual structures were initially optimized using the UHF/PM7 method (Unrestricted Hartree-Fock/Parametric Method 7) with the aim of reducing calculation time: DBSA, aniline, anilinium cation, $DBS^-$ anion, water, hydronium. These geometries were optimized using different charges (ranging from –2 to +2) and multiplicities, varying between singlet, doublet, triplet and quartet states according to the possibilities of each structure.

After optimization in the MOPAC software, the outputs were analyzed and the geometries of the structures were subjected to a second optimization using the Gaussian 03 software, with the DFT-B3LYP method (density functional theory-Becke, 3-parameter, Lee-Yang-Parr) using the 3-21G basis functions. Then, the geometries that presented lower energy for the same structures were subjected to the third stage of optimization using the DFT-B3LYP method, and the basis functions 6-311+G*, with the Gaussian 09 software.

The optimized geometries were used to construct the inputs for interactions between the studied structures, which were optimized with the Gaussian 03 software, and with the DFT-B3LYP method using the 3-21G basis functions.

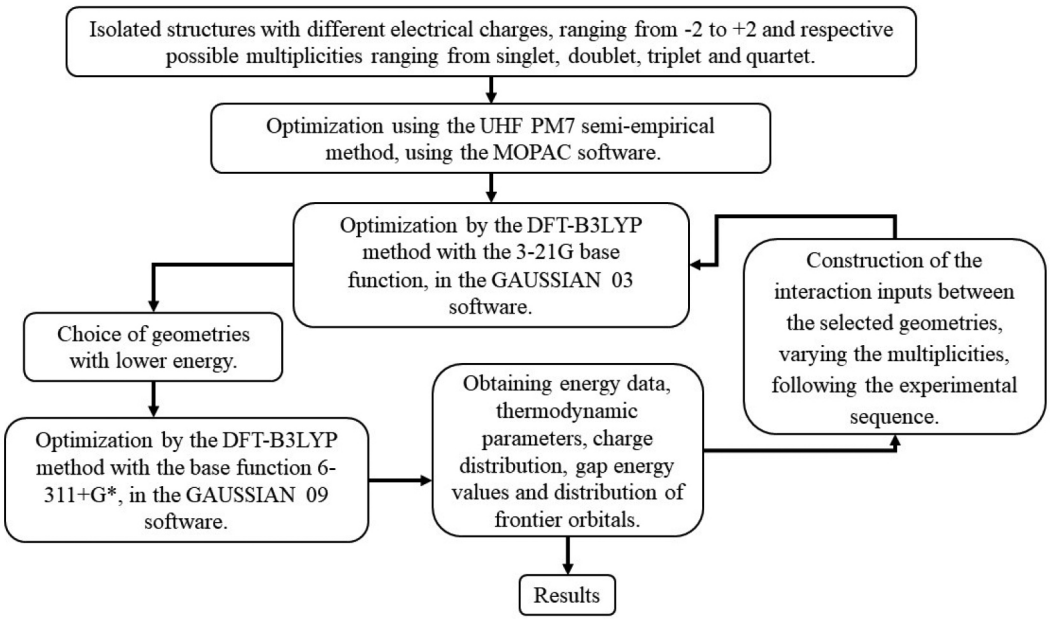


**Figure 1.** Scheme of the organization of molecular modeling.

Then, a second optimization was carried out applying the DFT-B3LYP method and the 6-311+G* basis functions, with the Gaussian 09 software. The geometries and their energies were obtained and subsequently analyzed, including the frontier orbitals and their energies and the distribution of charges on the structures. The construction of the interaction inputs followed a train of thought based on the synthesis procedure on the bench.

The positions of the water molecules were pre-fixed in all situations of the theoretical study based on the distribution of charges and frontier orbitals HOMO (highest occupied molecular orbital) and LUMO (lowest unoccupied molecular orbital) of the compounds involved. In each situation, the system formed by the interaction between the structures was called a "cluster".

## Results and Discussion

The analysis of the structures of the reactants, as well as the structures that can be found in equilibrium when dissolving the reactants in water, was carried out with the aim, from this information, to construct the necessary inputs for the next steps and monitor the evolution of the formation processes of the anilinium-DBS salt. The number of simulated water molecules varied from 0 to 5 due to the computational cost/time available to carry out the work.

### Calculation of energy changes and thermodynamic parameters

The energies of the clusters (of isolated structures and interactions) were calculated by the DFT-B3LYP method with the basis functions 6-311+G*. The energy change, ΔE, was calculated by the energy difference between the clusters: (*i*) containing all structures ($E_{(interaction)}$) and (*ii*) isolated structures ($\Sigma E_{i(specie\ i)}$), as shown generically in equation 1. The thermodynamic parameters ΔH (change in enthalpy), ΔS (change in entropy) and ΔG (change in Gibbs free energy) were calculated and are presented throughout the text.

$$\Delta E = E_{(interaction)} - \sum_{i=1}^{n} E_{i(specie\ i)} \quad (1)$$

### Steps in the synthesis of anilinium-DBS salt

#### Interaction with water molecules

The synthesis of anilinium-DBS salt was carried out in aqueous medium. To evaluate the effect of the solvent on modeling, the interactions of water with other structures were studied. To this end, the geometry of the structures of water ($H_2O$) and hydronium ($H_3O^+$) was optimized with different charges, ranging from –2 to +2, and multiplicities, from singlet to quartet, and are presented in Figure 2. The structures that presented the lowest energy were water with charge 0 (zero) and hydronium with charge +1 (positive one), both with singlet multiplicity. The HOMO orbitals in both structures are located perpendicular to the hydrogen plane, indicating that the nucleophilic action of water occurs through oxygen. LUMO orbitals are located throughout the molecular structure, except in the oxygen region, indicating that hydrogens act preferentially as electrophilic agents.

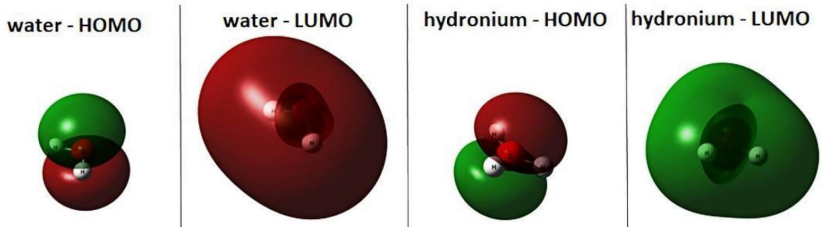


**Figure 2.** Representation of the optimized geometries of water and hydronium and their respective frontier orbitals. HOMO: highest occupied molecular orbital; LUMO: lowest unoccupied molecular orbital.

### DBSA dissolution and ionization

The DBSA structure that presented the lowest energy was optimized with singlet multiplicity and zero charge and served as a starting point for the calculation of frontier orbitals. The optimized DBSA geometry with its respective frontier orbitals is represented in Figure 3. Both orbitals, HOMO and LUMO, of the DBSA structure are located mainly on the aromatic ring and on the oxygens of the sulfonic group ($–SO_3H$). Based on these data, it is suggested that a possible interaction of DBSA with another species, such as the water molecule, will occur in the sulfonic group region.

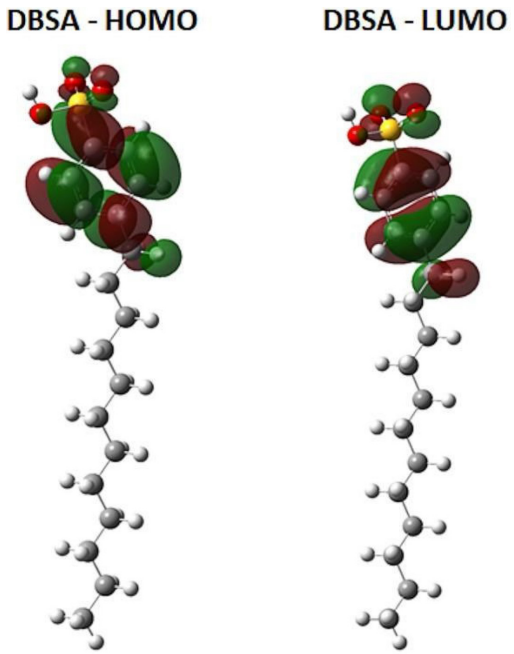


**Figure 3.** Representation of the optimized geometry and dodecylbenzene sulfonic acid (DBSA) frontier orbitals. HOMO: highest occupied molecular orbital; LUMO: lowest unoccupied molecular orbital.

The dissolution of DBSA in water and its ionization was evaluated, following the experimental procedure, represented in chemical equations 2 and 3. The calculated thermodynamic parameters indicate that DBSA ionization in aqueous media is an endothermic process, with decrease in entropy, resulting in a non-spontaneous transformation.

$$C_{18}H_{29}SO_3H_{(l)} \rightarrow C_{18}H_{29}SO_3H_{(aq)} \quad (2)$$

$$C_{18}H_{29}SO_3H_{(aq)} + H_2O_{(l)} \rightarrow C_{18}H_{29}SO^-_{3(aq)} + H_3O^+_{(aq)} \quad (3)$$

$\Delta E = 613..41$ kJ mol$^{-1}$; $\Delta H = 612.93$ kJ mol$^{-1}$

$\Delta S = –6.1379 \times 10^{-3}$ kJ mol$^{-1}$ K$^{-1}$; $\Delta G = 614.76$ kJ mol$^{-1}$

Based on the results of geometries and frontier orbitals of the DBSA, hydronium and water structures, presented in Figures 2 and 3, inputs were constructed with the interactions between the DBSA structure and the n water molecules, with n = 1, 2, 3, 4 and 5, as shown in Figure 4. The water molecules were positioned so that there was HOMO-LUMO interaction between the structures. The interaction charge was equivalent to the sum of the charges of the most stable structures, in this case 0 (zero), and the geometries were optimized with singlet and triplet multiplicities.

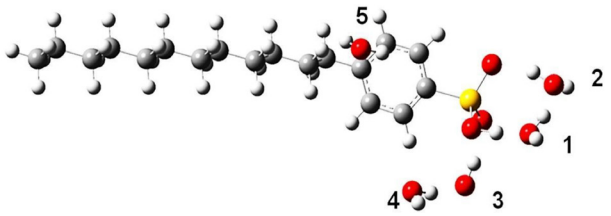


**Figure 4.** Representation of interaction inputs between the dodecylbenzene sulfonic acid (DBSA) structure and water molecules.

To evaluate the possible ionization of DBSA, the reaction was simulated in the opposite direction, since the modeling does not guarantee that the clusters optimized with the reactant structures form the products due to a possible potential barrier. This reaction is represented in equation 4. The initial geometries of interactions between the structure of DBSA and water were used, in which the transfer of hydrogen from DBSA to the water molecule in position 1 was induced, thus obtaining the interaction between the structures of the anion $DBS^–$ and of hydronium.

$$C_{18}H_{29}SO^-_{3(aq)} + H_3O^+_{(aq)} \rightarrow C_{18}H_{29}SO_3H_{(aq)} + H_2O_{(l)} \quad (4)$$

$\Delta E = –613.41$ kJ mol$^{-1}$; $\Delta H = –612.93$ kJ mol$^{-1}$

$\Delta S = +6.1379 \times 10^{-3}$ kJ mol$^{-1}$ K$^{-1}$; $\Delta G = –614.76$ kJ mol$^{-1}$

The geometries and frontier orbitals of the $DBS^-$ structure, and the clusters containing $DBS^-$, hydronium and water molecules after optimization, are represented in Figure 5, for better visualization. The frontier orbitals are represented in Figures S1 (HOMO) and S2 (LUMO), presented in Supplementary Information, SI section, as well as the values of the energy gap. The geometries presented refer to clusters with lower energy in relation to the multiplicity, in this case the singlet state. The geometries of interactions between the structures of $DBS^-$, hydronium and n waters converged to form the structure of DBSA and (n + 1) water molecules. The distances between the structures in these clusters were compared with the geometries obtained in the optimized clusters containing DBSA and water molecules and the differences were not significant (less than 0.001 Å, and in some cases the values were the same). We assume that the results of the DBSA.$(n + 1)H_2O$ interaction and the $DBS^-H_3O^+.nH_2O$ interaction are the same.

In the $DBS^-$ structure, the HOMO orbital is in the sulfonic group. With the interaction between $DBS^-$ and hydronium, which converged to form DBSA and water, this orbital partially moved to the aromatic ring and extended to the alkyl chain as water molecules were added. The LUMO orbital was in the methyl group present at one of the ends of the alkyl chain in the $DBS^-$ structure. In the interactions that converged to form DBSA and water, the LUMO moved towards the ring and the sulfonic group. The value of the energy gap in the $DBS^-$ anion structure is smaller than that of the interaction between the DBSA and water structures, respectively 327.67 and 570.88 kJ $mol^{-1}$. The energy gap in each structure is associated with its stability, that is, a higher value of the energy gap in interaction, in relation to the isolated structure indicates that the interaction increases the stability of the cluster.[50,51] The energy gaps between interactions with different amounts of water present values in the range of 568.93 to 574.16 kJ $mol^{-1}$, suggesting that the solvation process increases the stability of DBSA in relation to the ionized form, $DBS^-$. The results of the energy changes of the DBSA.$(n + 1)H_2O$ and $DBS^-H_3O^+.nH_2O$ interactions are presented in Figure 6, which refer to the interactions presented in Figure 5 and were calculated according to equations 5 and 6, where n represents the number of water molecules, varying from 1 to 5. In the calculations of energy changes, the final state is the same in both situations, and the final energy is the energy of the DBSA.$nH_2O$ interactions, while the energy of the initial state is given by the sum of the individual energies of the species that will interact (DBSA and $nH_2O$; DBSA, $H_3O^+$ and $nH_2O$). The energy changes values obtained were –70.12, –136.00, –148.94, –211.53 and –221.43 kJ $mol^{-1}$, for the DBSA.$(n + 1)H_2O$ system, and –678.45, –743.00, –755.27, –817.86 and –827.76 kJ $mol^{-1}$, for $DBS^-$-$H_3O^+.nH_2O$. It was observed that the negative changes were greater in the $DBS^-$-$H_3O^+.nH_2O$ interactions. As the final states are the same, the greatest energy change will be associated with the initial state with the highest energy, that is, the interactions in the $DBS^-$-$H_3O^+.nH_2O$

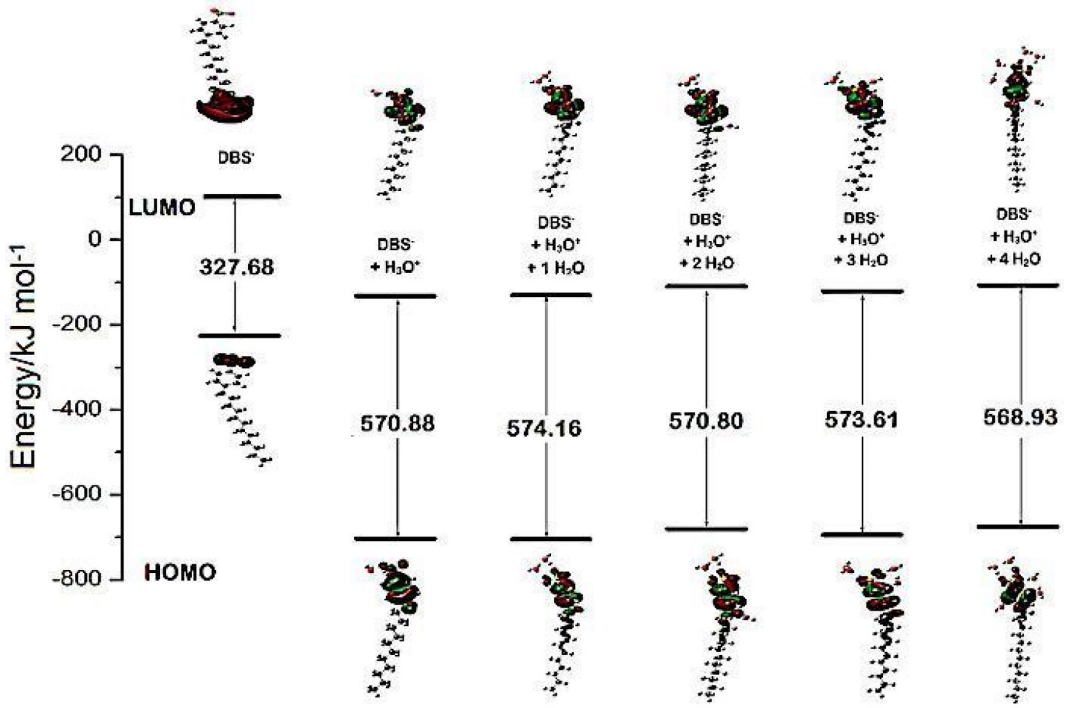


**Figure 5.** Representation of the geometries, frontier orbitals and energy gaps, obtained for the DBS-structures (dodecylbenzene sulfonate-structures) and the interactions between $DBS^-$ hydronium and water molecules.

cluster have higher energy than the DBSA.(n + 1)$H_2O$ interactions, thus being more unstable, indicating that DBSA.n$H_2O$ interactions are more favorable. The data indicate that the solubilization of DBSA in an aqueous medium is energetically favorable and is compatible with the experimental observation that this is a relatively weak acid, p$K_a$ = +2.55,[52] not easily ionizing in the presence of water, but soluble in water.

$$\Delta E(DBSA.(n + 1)H_2O) = E(DBSA.(n + 1)H_2O) - ((n + 1) \times E(H_2O) + E(DBSA)) \quad (5)$$

$$\Delta E(DBS^- H_3O^+.nH_2O) = E(DBSA.nH_2O) - (n \times E(H_2O) + E(H_3O^+) + E(DBS^-)) \quad (6)$$

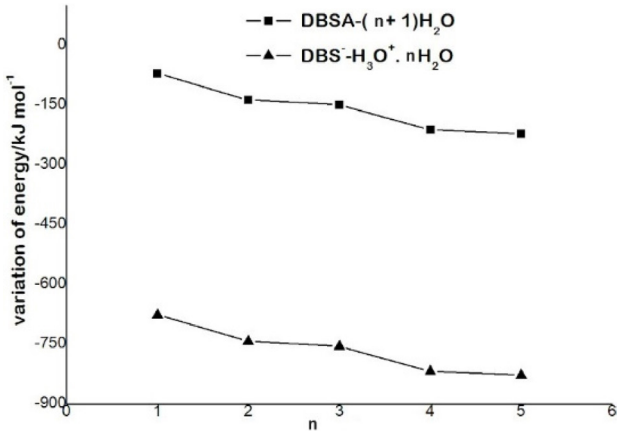


**Figure 6.** Variation of energy (ΔE) graph of the interactions between the DBSA and $DBS^-/H^+$ structures with n water molecules. DBSA: dodecylbenzene sulfonic acid; DBS: dodecylbenzene sulfonate.

The charge distribution in the DBSA.n$H_2O$ interaction was also evaluated, whose values are shown in Table 1. The first column indicates the structures contained in the cluster, and the columns named $\delta_{nH_2O}$ / e and $\delta_{DBSA}$ / e represent the charges, the n water molecules and DBSA, in elementary charge units respectively. The values represent the sum of the atomic charges of each structure present in the outputs. The charges on the water and DBSA structures presented values that converge on neutrality. The inputs initially contained the structures of $DBS^-$ and hydronium ions, which converged to form the structures of DBSA and water, both with a neutral charge, indicating that this is a weak acid, not ionizing easily, confirming the data of previous ones.

**Table 1.** Charge distribution in interactions between DBSA and water

| Structure | $\delta_{nH_2O}$ / e | $\delta_{DBSA}$ / e |
|---|---|---|
| DBSA + 1$H_2O$ | 0.008 | –0.008 |
| DBSA + 2$H_2O$ | 0.015 | –0.015 |
| DBSA + 3$H_2O$ | –0.013 | 0.013 |
| DBSA + 4$H_2O$ | 0.004 | –0.004 |
| DBSA + 5$H_2O$ | –0.012 | 0.012 |

DBSA: dodecylbenzene sulfonic acid; δ: charge distribution; e: elementary charge; n: number of water molecules.

### Dissolution and aniline ionization

The geometry of the aniline molecule, optimized with singlet multiplicity and zero charge, and its HOMO and LUMO orbitals are represented in Figure 7. LUMO is in the aromatic ring, consequently, this is the region that will act as an electrophile. It is observed that the HOMO orbital is located throughout the molecular structure. However, as there is an overlap of the HOMO-LUMO orbitals in the ring region, the amine group will preferentially act as a nucleophile.

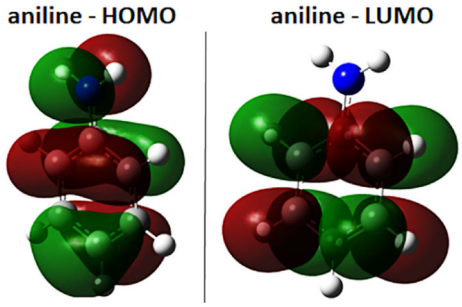


**Figure 7.** Representation of the optimized geometry and frontier orbitals of aniline. HOMO: highest occupied molecular orbital; LUMO: lowest unoccupied molecular orbital.

The PAni synthesis mechanism, independent of the oxidizing agent and acid used, indicates the ionization of aniline in the presence of acid in an aqueous medium, forming the respective aniline salt.[53] Based on these data, at this stage, its ionization in an acidic medium, forming the anilinium cation, represented in Figure 8, were evaluated. The calculated thermodynamic parameters indicate that the formation of the anilinium ion through the reaction of aniline with the hydronium ion is an exothermic process, with decrease in entropy, resulting in a spontaneous transformation.

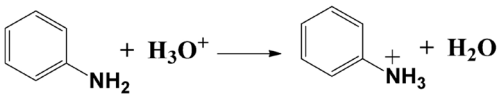


$\Delta E = -191.02$ kJ mol$^{-1}$; $\Delta H = -191.02$ kJ mol$^{-1}$

$\Delta S = -6.3726 \times 10^{-1}$ kJ mol$^{-1}$ K$^{-1}$; $\Delta G = -190.83$ kJ mol$^{-1}$

**Figure 8.** Chemical equation for the formation of the anilinium cation (adapted from reference 54).

The inputs for the interaction between the structures of hydronium and aniline and water molecules, represented in Figure 9, were constructed so that the HOMO of aniline

was facing the LUMO region of hydronium and water molecules. The inputs were constructed by simulating the interaction between aniline, hydronium and n water molecules, with n varying from 0 to 4, and were named as aniline-$H_3O^+$.n$H_2O$. The interaction charge was equivalent to the sum of the charges of the most stable structures, in this case, +1 (positive one), and the clusters were optimized with singlet and triplet multiplicities.

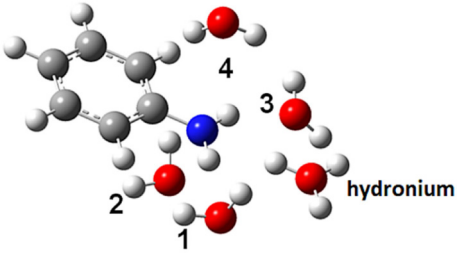


**Figure 9.** Representation of the interaction geometries between the structure of aniline, hydronium and water molecules.

The optimized geometries and frontier orbitals of the aniline-$H_3O^+$.n$H_2O$ system are represented in Figure 10, the frontier orbitals are represented in Figures S3 (HOMO) and S4 (LUMO), SI section, for better visualization. The geometries with the lowest energy and singlet multiplicity are shown. It is observed that the energy gap of the interaction between the aniline and hydronium structures is smaller than the energy gap of isolated aniline, 136.19 and 507.62 kJ mol$^{-1}$, respectively. The energy gap of the aniline-$H_3O^+$ structure presented a lower value than those of the interactions between the structures of aniline, hydronium and water molecules. The HOMO orbital is in the aniline structure, while the LUMO orbital is in the hydronium structure. In the geometries of aniline-$H_3O^+$.n$H_2O$ interactions, in those that contained 1 and 4 water molecules in the inputs, there was transfer of a hydrogen from hydronium to aniline, forming anilinium and another water molecule. These interactions presented higher energy gaps, of 618.59 and 627.56 kJ mol$^{-1}$ respectively, compared to the gaps of 573.17 and 582.40 kJ mol$^{-1}$ of the interactions that contained 2 and 3 water molecules. When evaluating the interaction distance between the hydrogen of the hydronium closest to the aniline structure in each interaction, it was observed that the largest value, 1.70 Å, corresponds to the interaction with n = 2, and the smallest value, 1.07 Å, for the interaction with n = 4. This indicates that the formation of anilinium is associated with an increase in band gap energy and the consequent stabilization of the system. The HOMO orbitals in interactions with n = 2 and 3 were formed in the structures of aniline and hydronium, while LUMO was formed in the aromatic ring of aniline. In clusters with n = 1 and 4, in which there was a transfer of hydrogen from hydronium to aniline, the HOMO and LUMO orbitals are in the structure of the anilinium formed.

As not all results converged to the formation of anilinium, the geometries and frontier orbitals of the reaction were analyzed in the opposite direction, represented in equation 7. The geometries were obtained by inducing the transfer of a hydrogen atom from hydronium to aniline at the interaction inputs, which were then optimized. The lowest energy results were those that had singlet state multiplicity as a parameter, which are shown in Figure 11, and the frontier orbitals are represented in

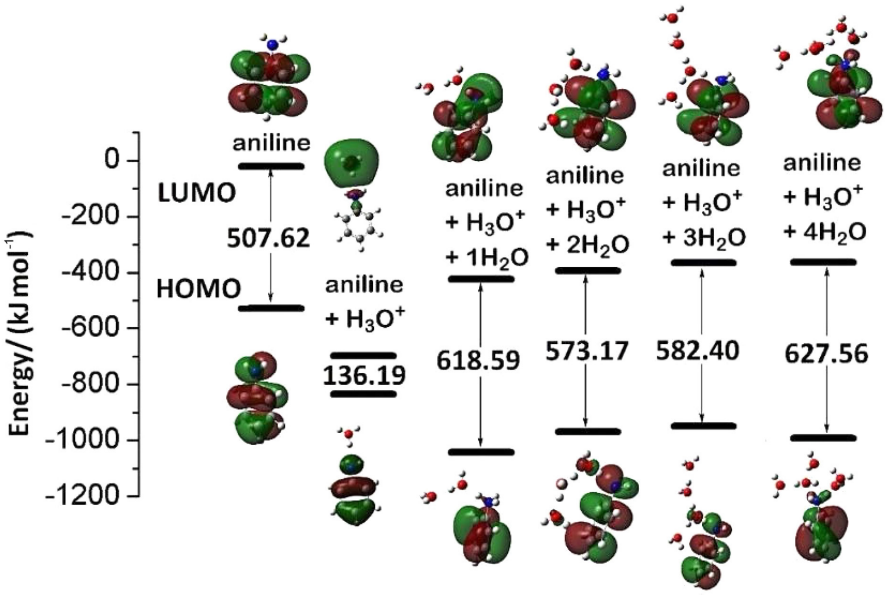


**Figure 10.** Representation of geometries and frontier orbitals (HOMO above and LUMO below) of aniline structure, and the structures resulting in the study of interactions between aniline, hydronium and water molecules. HOMO: highest occupied molecular orbital; LUMO: lowest unoccupied molecular orbital.

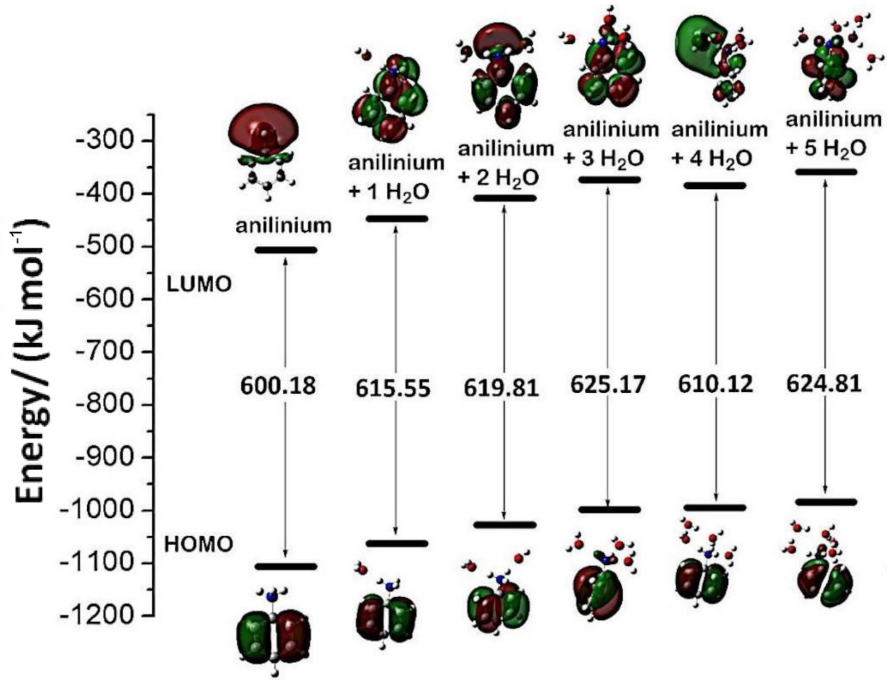


**Figure 11.** Representation of the geometries and frontier orbitals of interactions between anilinium structures and water molecules. HOMO: highest occupied molecular orbital; LUMO: lowest unoccupied molecular orbital.

Figures S5 (HOMO) and S6 (LUMO), SI section, for better visualization. In the interactions between anilinium and water, it was observed that there was no change in the configuration of the structures. The energies gap presented values in the range of 610.11 to 625.17 kJ mol$^{-1}$, closer to the values observed in the aniline-$H_3O^+$.n$H_2O$ interactions that converged to the formation of anilinium (Figure 10), and greater than that of the isolated structure, which presented an energy gap of 600.18 kJ mol$^{-1}$.

$$C_6H_5NH^+_{3(aq)} + H_2O \rightarrow C_6H_5NH_2 + H_3O^+ \quad (7)$$

$\Delta E$ = 191.02 kJ mol$^{-1}$; $\Delta H$ = 191.02 kJ mol$^{-1}$

$\Delta S = 6.3726 \times 10^{-1}$ kJ mol$^{-1}$ K$^{-1}$; $\Delta G$ = 190.83 kJ mol$^{-1}$

Comparing the geometries of the structures presented in Figures 10 and 11, the tendency to form anilinium when aniline is solubilized in an acidic medium is observed. The data obtained by analyzing the location of the frontier orbitals and the energy gaps indicate that the clusters made up of anilinium and water molecules have greater stability than their precursors.

The results of the energy changes in the interactions between the aniline, hydronium and water structures and in the interactions between the anilinium and water structures are presented in Figure 12, which refer to the interactions presented in Figures 10 and 11 and were calculated according to equations 8 and 9. In the equations, n = (hydronium + water) in the interactions.

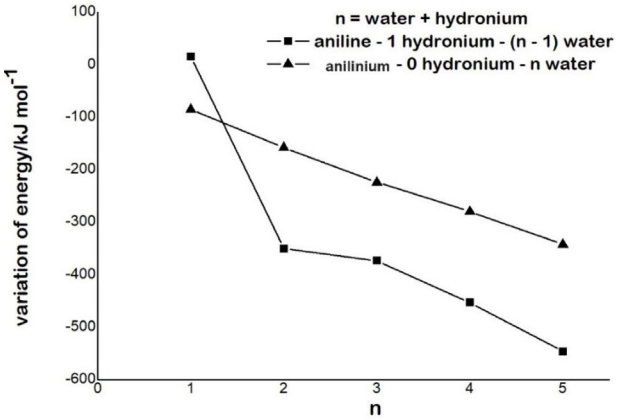


**Figure 12.** Graph of the relationship between variation of energy ($\Delta E$) of interactions: between the structures of aniline, hydronium and water; and between the structures of anilinium and water, and the number of water molecules.

$$\Delta E(\text{aniline-}H_3O^+.(n-1)H_2O) = E(\text{aniline-}H_3O^+.nH_2O) - ((n-1) \times E(H_2O) + E(H_3O^+) + E(\text{aniline})) \quad (8)$$

$$\Delta E(\text{anilinium}.nH_2O) = E(\text{anilinium}.nH_2O) - (n \times E(H_2O) + E(\text{anilinium})) \quad (9)$$

The energy changes in the interactions between the anilinium and water structures were –84.60, –157.63, –223.58, –279.65 and –342.17 kJ mol$^{-1}$, in relation to the isolated structure of anilinium, and an increase in the negative change of $\Delta E$ was observed. The energy change in the interaction between the aniline and hydronium structures in relation to isolated aniline was +15.82 kJ mol$^{-1}$, indicating an energetically unfavorable transformation. A decrease

in the difference in energy change values between the interactions aniline-$H_3O^+$.(n – 1)$H_2O$ and anilinium-n$H_2O$, n = 3 and 4, is observed, precisely in the interactions where there were no transfer of the hydronium proton to the aniline in aniline-$H_3O^+$.(n – 1)$H_2O$ interactions, indicating that the transfer is an energetically favorable process. These data indicate that the anilinium formation process in an acidic environment is energetically favorable.

In order to evaluate the charge transfer in interactions, the charges on the structures were analyzed, and the results are presented in Table 2. The columns named $\delta_{aniline}$ / e, $\delta_{nH_2O}$ / e, $\delta_{H_3O^+}$ / e and $\delta_{anilinium}$ / e present the charges values, in the respective aniline-$H_3O^+$.(n – 1)$H_2O$ interactions. The columns named $\delta_{nH_2O}$ / e and $\delta_{aniline}$ / e present the values of the charges in the anilinium and water structures, in the anilinium-n$H_2O$ interactions, in elementary charge units and (1e = 1.6 × $10^{-19}$ C). Empty fields indicate that the column-related structure is not present in the analyzed output.

**Table 2.** Charge distribution of the structures in the outputs of the interactions between aniline, hydronium and water, and the interactions between anilinium and water

| n | Aniline-$H_3O^+$.(n – 1)$H_2O$ | | | | Anilinium-n$H_2O$ | |
|---|---|---|---|---|---|---|
| | $\delta_{aniline}$ / e | $\delta_{nH_2O}$ / e | $\delta_{H_3O^+}$ / e | $\delta_{anilinium}$ / e | $\delta_{anilinium}$ / e | $\delta_{nH_2O}$ / e |
| 1 | 0.021 | – | 0.979 | – | 0.991 | 0.009 |
| 2 | – | 0.022 | – | 0.978 | 1.001 | –0.001 |
| 3 | –0.064 | 0.174 | 0.890 | – | 1.022 | –0.022 |
| 4 | –0.058 | 0.060 | 0.998 | – | 1.002 | –0.002 |
| 5 | – | 0.049 | – | 0.951 | 1.005 | –0.005 |

δ: charge distribution; e: elementary charge; n: number of water molecules.

In the interactions between aniline-$H_3O^+$.(n – 1)$H_2O$ with n = 2 and 5, the transfer of a proton from hydronium to aniline was observed and the charge in the formed structure, anilinium, converged to +1e. In interactions with n = 1, 3 and 4, there were no proton transfer from hydronium to aniline, and positive charge density values were found in hydronium with values close to +1e. In the interactions between anilinium-n$H_2O$, the charges in the anilinium structure presented values that converge to +1e. The data indicate that, once anilinium is formed in the cluster, its charge will be +1e, suggesting that aniline in an acidic medium remains in the protonated form, as described in the literature.[54]

### Formation of anilinium-DBS salt

At this stage, the formation of anilinium-DBS salt was evaluated, according to the reaction represented in equation 10. The calculated thermodynamic parameters indicate that the formation of the anilinium-DBS salt through the reaction of aniline with the dodecylbenzene sulfonic acid is an endothermic process, with increase in entropy, resulting in a spontaneous transformation.

$$C_6H_5NH_{2(aq)} + C_{18}H_{29}SO_3H_{(aq)} \rightarrow C_6H_5NH_3(C_{18}H_{29}SO_3)_{(s)} \quad (10)$$

$\Delta E$ = 40.44 kJ $mol^{-1}$; $\Delta H$ = 37.26 kJ $mol^{-1}$

$\Delta S$ = 131.86 J $mol^{-1}$ $K^{-1}$; $\Delta G$ = –2.051 kJ $mol^{-1}$

The inputs for the interaction between the structures of DBSA, aniline and m water molecules, being m = 0, 1, 2, 3, 4, 5, were constructed using the geometries of DBSA and aniline optimized in the previous steps, and interact with the HOMO regions of the DBSA structure with the LUMO regions of the water and aniline structures, whose structures are shown in Figure 13. The water molecules were positioned to enable the evaluation of the influence of the solvent interaction in some regions close to the aniline and DBSA structures. The interaction charge was equivalent to the sum of the charges of the most stable structures, in this case 0 (zero), and the optimizations were carried out with singlet and triplet state multiplicities.

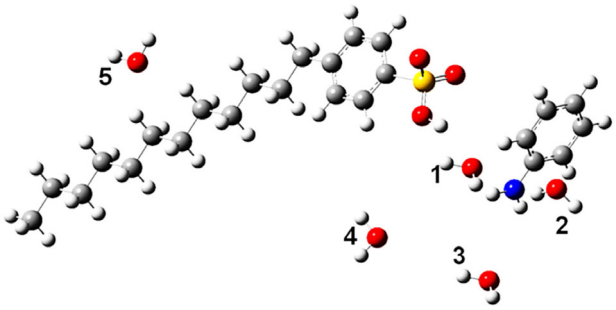


**Figure 13.** Representation of the geometries of interaction inputs between the structures of aniline, dodecylbenzene sulfonic acid (DBSA) and water molecules.

Figure 14 presents the results obtained by combining the frontier orbitals of aniline and DBSA, indicating on the left the aniline-DBSA interaction and on the right, the structure of the anilinium-DBS salt. It is observed that the aniline structure presents higher HOMO and LUMO energy values than DBSA. This means that when these two structures interact, the higher HOMO energy value of aniline indicates its greater electron-donor character when compared to DBSA. Likewise, the lower LUMO energy value of DBSA indicates its greater ability to accept electrons when compared to aniline. This behavior suggests that aniline can donate electrons to abstract a hydrogen atom from the sulfonic group of DBSA, while the DBSA structure can accept the electron resulting from the formation of this $H^+$ ion. When comparing the gap energy values of the aniline-DBSA interaction, 491.79 kJ $mol^{-1}$, with the value of the anilinium-DBS structure, 507.00 kJ $mol^{-1}$, an increase

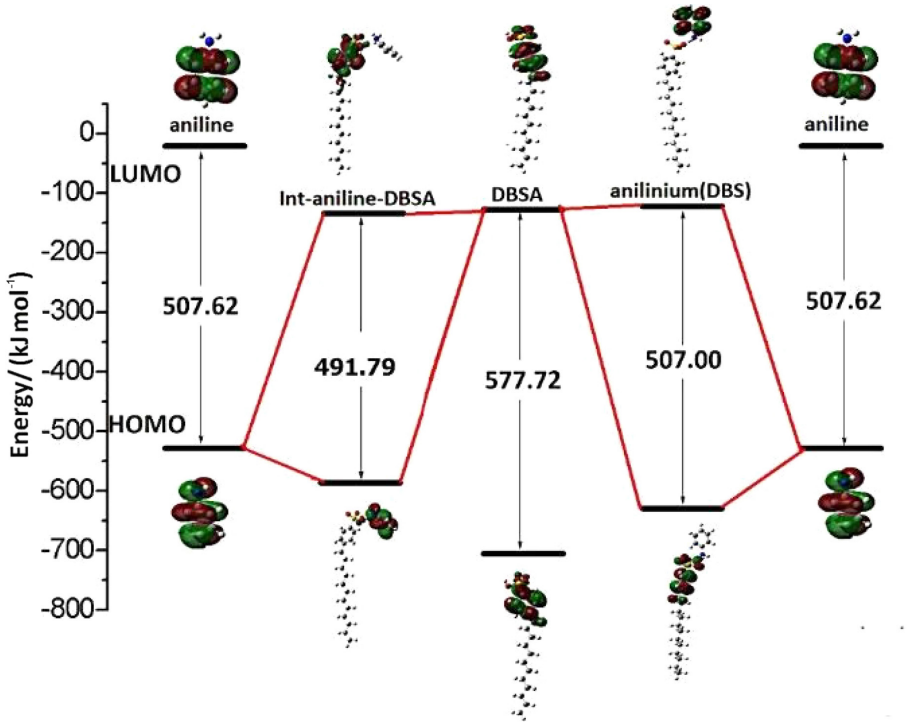


**Figure 14.** Representation of the results of combining the frontier orbitals of the aniline and dodecylbenzene sulfonic acid (DBSA) structures.

in the gap energy can be seen, indicating an increase in the stability of the structure. These results are consistent with the experimentally verified anilinium-DBS salt formation mechanism.[55,56]

In Figure 15 the optimized geometries and frontier orbitals of the interactions between aniline, DBSA and water are represented. The frontier orbitals are represented in Figures S7 (HOMO) and S8 (LUMO), SI section, for better visualization. The geometries refer to the interactions that present lower energy in relation to the singlet multiplicity. It was observed that there was a transfer of a hydrogen atom from the sulfonic group of DBSA to the amino group of aniline in interactions with m = 1, 2, 3 and 4. The interactions presented gap energy in the range of 506.79 to 533.91 kJ $mol^{-1}$, except for the interaction with 5 water molecules, which presented a gap energy of 422.16 kJ $mol^{-1}$. This result may be associated with the presence of a water molecule interacting with the alkyl group of DBSA, indicating that this region is hydrophobic. The HOMO orbitals in interactions with m = 0 and 5 are mainly located in the aniline structure. In the other interactions, the HOMO orbitals are in the sulfonic group and in the aromatic ring of $DBS^-$, indicating that negative charges are concentrated in this region in interactions with m = 0 and 5, the opposite pattern was observed for the LUMO orbitals. These are mainly located in the sulfonic group and aromatic ring of DBSA. In the other interactions, the LUMO orbitals are in the anilinium structure, indicating that there is a concentration of positive charges, compatible with the formation of the anilinium-DBS salt. The inversion of the location of the frontier orbitals indicates changes in the reactivity characteristics, alternating the role of the structures as nucleophile and electrophile.

Since hydrogen transfer was not observed in interactions with m = 0 and 5, the reaction was simulated in the opposite direction, represented in equation 11. For this, interaction inputs between anilinium, $DBS^-$ and water were constructed. These geometries were obtained by inducing the transfer of a proton from DBSA to the aniline structure, forming the anilinium ion, at the inputs of the interaction between aniline, DBSA and water. The inputs were optimized, and the frontier orbitals were calculated.

$$C_6H_5NH_3(C_{18}H_{29}SO_3)_{(s)} \rightarrow C_6H_5NH_{2(aq)} + C_{18}H_{29}SO_3H_{(aq)} \quad (11)$$

$\Delta E = -40.44$ kJ $mol^{-1}$; $\Delta H = -37.26$ kJ $mol^{-1}$

$\Delta S = -131.86$ J $mol^{-1}$ $K^{-1}$; $\Delta G = 2.051$ kJ $mol^{-1}$

The results of the anilinium-$DBS^-$.m$H_2O$ interactions are presented in Figure 16, the frontier orbitals are represented in Figures S9 (HOMO) and S10 (LUMO), SI section, for better visualization. The geometries refer to the interactions that present lower energy and singlet multiplicity. The optimized geometries and the location of the frontier orbitals resemble those of the interactions between aniline and DBSA in which anilinium-$DBS^-$ was formed (see Figure 14). The interactions between

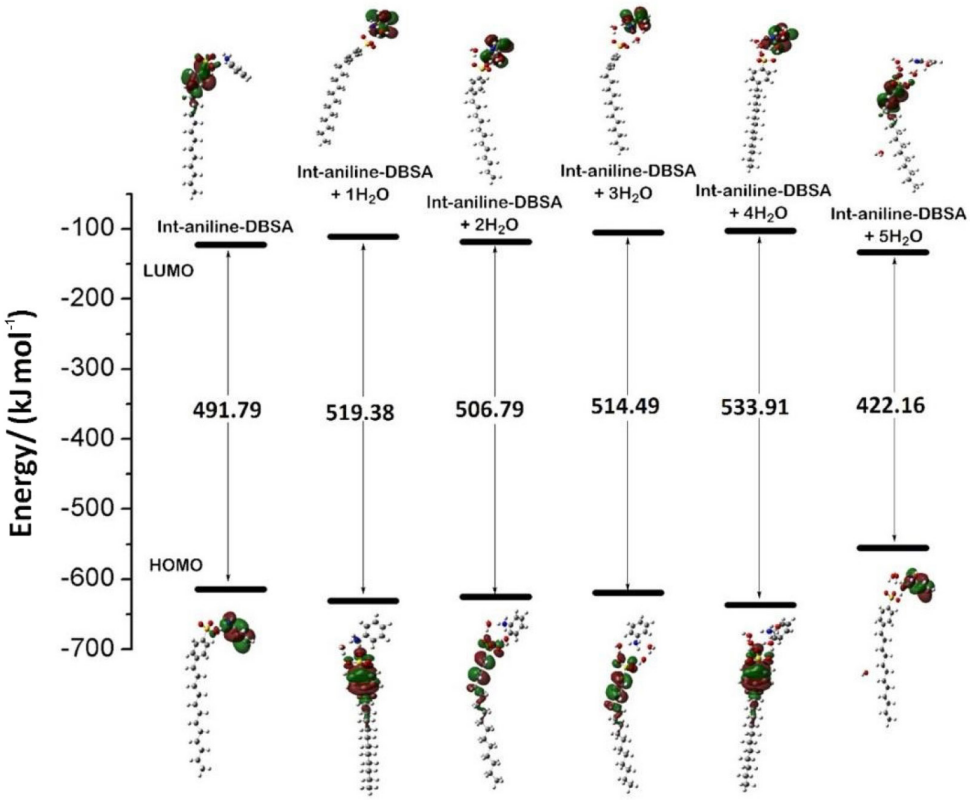


**Figure 15.** Representation of the geometries and frontier orbitals (HOMO above and LUMO below) of the interaction between the structures of dodecylbenzene sulfonic acid (DBSA), aniline and water molecules. HOMO: highest occupied molecular orbital; LUMO: lowest unoccupied molecular orbital.

anilinium-$DBS^-.mH_2O$ with m = 3, 4 and 5, presented higher energy gap when compared to the interactions between aniline and DBSA with the same amounts of water (Figure 15), indicating that the salt structure is more stable than that of DBSA and aniline. In the anilinium-$DBS^-.mH_2O$ system, the energy gap values varied depending on the region where the water molecule interacts, and when comparing an interaction with the one immediately preceding, a decrease is observed when the water structure is placed close to one of the oxygen atoms of the sulfonic group (m = 2) and close to the alkyl group (m = 5) indicating a decrease in the stability of the cluster. The decrease in gap energy with the presence of a water molecule in the sulfonic group region suggests that the nucleophilic action of this group moves to the oxygen region that interacts directly with anilinium, reducing the interaction in the region of other oxygen atoms. The decrease in gap energy when a water molecule is added to the alkyl group region (m = 5) suggests that this region is hydrophobic. These results indicate the formation of anilinium and $DBS^-$ structures, as they are the most stable structures when compared to DBSA and aniline. As the hydrophobic alkyl group corresponds to a relatively large fraction of the molecule, the result indicates that the salt formed is poorly soluble in water, as observed experimentally.

The results of the energy changes of the interactions between the structures in the aniline-DBSA.$mH_2O$ and anilinium-$DBS^-.mH_2O$ systems are shown in Figure 17, which refer to the interactions presented in Figures 15 and 16 and were calculated according to the equations 12 and 13, where m represents the number of water molecules.

$$\Delta E(\text{anilinium-DBS}^-.mH_2O) = E(\text{anilinium} - \text{DBS}^-.mH_2O) - (m \times E(H_2O) + E(\text{anilinium}) + E(\text{DBS}^-)) \quad (12)$$

$$\Delta E(\text{aniline-DBSA}.mH_2O) = E(\text{aniline} - \text{DBSA}.mH_2O) - (m \times E(H_2O) + E(\text{DBSA}) + E(\text{aniline})) \quad (13)$$

The energy changes of the aniline-DBSA.$mH_2O$ interactions were –71,70, –139.37, –188.67, –239.79, –307.83 and –276.26 kJ $mol^{-1}$, for m = 0, 1, 2, 3, 4 and 5 respectively, compared to their respective isolated structures. It was found that these values intensify with the addition of water molecules to the cluster, except when the interaction includes five water molecules. The change in positive energy from m = 4 to m = 5 is associated with the non-transfer of hydrogen from DBSA to aniline. In the other interactions, the energy change was negative, indicating that aniline and DBSA interact spontaneously to form the anilinium-DBS salt. The energy changes for the anilinium-$DBS^-.mH_2O$ system were –462.71, –546.70,

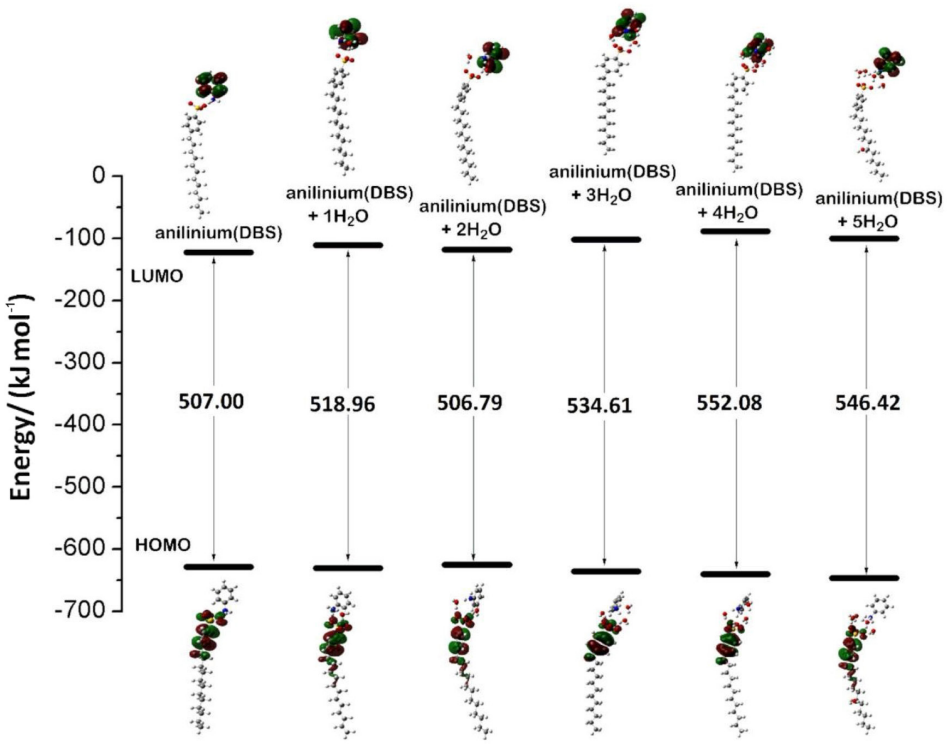


**Figure 16.** Representation of the geometries and frontier orbitals of the interaction between the structures of $DBS^-$, anilinium and water molecules. DBS: dodecylbenzene sulfonate.

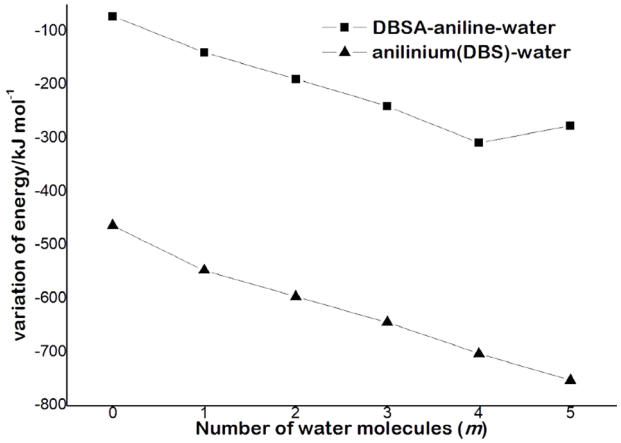


**Figure 17.** Graph of the relationship between variation of energy (ΔE) of aniline-DBSA-water and anilinium-$DBS^-$.$mH_2O$ interactions.

–595.93, –643.78, –702.80 and –752.60 kJ $mol^{-1}$, for m = 0, 1, 2, 3, 4 and 5 respectively, in relation to the respective isolated structures. These changes are more negative than those in aniline-DBSA.$mH_2O$ interactions. These data indicate that the formation of anilinium-DBS is favored in an aqueous medium.

The charge distribution in the structures resulting in the aniline-DBSA.$mH_2O$ and anilinium-$DBS^-$.$mH_2O$ interactions were also evaluated. The results are presented in Table 3, expressed in elementary charge units and (1e = 1.6 × $10^{-19}$ C) and identified as $\delta_{aniline}$ / e, $\delta_{nH_2O}$ / e, $\delta_{DBSA}$ / e, $\delta_{anilinium}$ / e and $\delta_{DBS^-}$ / e. The values at the top of the table refer to the aniline-DBSA.$mH_2O$ system, and at the bottom, to the anilinium-$DBS^-$.$mH_2O$ system. Fields in which no values appear indicate that the structure was not present in the analyzed output. In the structures in

**Table 3.** Result of charge distribution in the interaction between aniline, DBSA and the m water molecules (top), in the interaction between the $DBS^-$ and anilinium ions and the m water molecules (bottom)

| m | Aniline-DBSA.$mH_2O$ | | | | |
|---|---|---|---|---|---|
| | $\delta_{aniline}$ / e | $\delta_{mH_2O}$ / e | $\delta_{DBSA}$ / e | $\delta_{anilinium}$ / e | $\delta_{DBS^-}$ / e |
| 0 | –0.029 | – | 0.029 | – | – |
| 1 | – | 0.010 | – | 0.878 | –0.888 |
| 2 | – | 0.052 | – | 0.907 | –0.959 |
| 3 | – | –0.069 | – | 1.015 | –0.946 |
| 4 | – | –0.059 | – | 0.630 | –0.571 |
| 5 | –0.004 | 0.018 | 0.014 | – | – |
| m | Anilinium-$DBS^-$.$mH_2O$ | | | | |
| | $\delta_{aniline}$ / e | $\delta_{mH_2O}$ / e | $\delta_{DBSA}$ / e | $\delta_{anilinium}$ / e | $\delta_{DBS^-}$ / e |
| 0 | – | – | – | 0.340 | –0.340 |
| 1 | – | 0.012 | – | 0.884 | –0.896 |
| 2 | – | 0.038 | – | 0.907 | –0.945 |
| 3 | – | 0.056 | – | 0.914 | –0.970 |
| 4 | – | 0.104 | – | 0.904 | –1.008 |
| 5 | – | 0.105 | – | 0.857 | –0.962 |

DBS: dodecylbenzene sulfonate; DBSA: dodecylbenzene sulfonic acid; δ: charge distribution; e: elementary charge; n: number of water molecules.

which there were a proton transfer from DBSA to aniline, forming anilinium and $DBS^-$ (m = 1, 2, 3 and 4 at the top of the table) and in the interactions between anilinium and $DBS^-$, the distribution of a positive charge in anilinium and a negative one in DBS was observed. The convergence of the charge distribution for |1e| showed dependence on the presence of water molecules. The data presented in this step suggest that the structures of aniline and DBSA ionize when solubilized together in an aqueous medium. This ionization leads to the formation of anilinium-DBS salt. Experimentally, it was observed that a gelatinous solid white salt forms in the reaction medium.

### Experimental results

To evaluate the results of molecular modeling, the vibrational spectra in the mid-infrared region of DBSA, aniline, and gelatinous solid white salt were experimentally obtained. The absorptions were analyzed and compared with the objective of evaluating whether the salt formed was anilinium (DBS), as predicted by molecular modeling. The results are presented in Figure S11, SI section. The experimental absorptions in the spectra are presented in Table S1, SI section.

The band at 3375 $cm^{-1}$, attributed to stretching of the O–H bond of the sulfonic group, appears only in the DBSA spectrum. The peaks at 3428 and 3351 $cm^{-1}$, attributed to symmetric and asymmetric stretching of the N–H bond in the $–NH_2$ group, appear only in the aniline spectrum. The broad band around 3116 $cm^{-1}$, attributed to stretching of the $–NH_3^+$ group, combined with the peak at 1537 $cm^{-1}$, associated with the angular deformation of this group, are observed only in the salt spectrum. It is observed that the peaks referring to the other groups in aniline and DBSA are also observed in the salt, indicating that there was a change in the assignments of the amino and sulfonic groups. These data suggest the formation of the anilinium-DBS salt, as predicted by molecular modeling and in agreement with the literature.[24,53,54]

## Conclusions

Using molecular modeling methods, it was possible to correlate the main parameters related to the interaction between the structures of aniline, DBSA (dodecylbenzene sulfonic acid) and water molecules: energy changes, frontier orbitals, gap energy, charge distribution and thermodynamic parameters. The change in energy and in Gibbs free energy results indicated that DBSA solubilizes in water, but the ionization with the formation of hydronium ions is not favorable. This result is consistent with experimental data, which indicate that DBSA is a weak acid. Regarding aniline, the results showed that its solubilization in water is facilitated in the presence of hydronium ion, which is also verified experimentally. In the aniline-DBSA system, the results of the interactions between the frontier orbitals showed that aniline acts as an electron donor and DBSA as an electron acceptor, which is consistent with the formation of the anilinium cation and the $DBS^-$ (dodecylbenzene sulfonate) anion. The band gap energy values showed that the anilinium-DBS structure is more stable than the aniline-DBSA one. The energy changes in the anilinium-$DBS^-.mH_2O$ interactions depend on the position of the water molecules, which influences the solubility of this system. All results obtained through molecular modeling agree with experimental data on the formation of anilinium-DBS salt.

## Supplementary Information

Complementary information (frontier orbitals representation, output of thermodynamic parameter calculations using Gaussian 09, infrared spectroscopy data and reference) is freely available at https://jbcs.sbq.org.br/ as a PDF file.

## Acknowledgments

The authors would like to thank Fundação de Amparo à Pesquisa do Estado de Goiás (FAPEG) for granting the scholarship. The authors also thank Centro de Análises, Inovação e Tecnologia em Ciências Naturais e Aplicadas (CAITEC) da Universidade Estadual de Goiás (UEG).

## References

1. Liu, P.; Yan, J.; Guang, Z.; Huang, Y.; Li, X.; Huang, W.; *J. Power Sources* **2019**, *424*, 108. [Crossref]
2. Zhang, Y.; Duan, Y.; Liu, J.; *Spectrochim Acta, Part A* **2017**, *171*, 305. [Crossref]
3. Ashokan, S.; Ponnuswamy, V.; Jayamurugan, P.; Chandrasekaran, J.; Subba Rao, Y.; *Superlattices Microstruct.* **2015**, *85*, 282. [Crossref]
4. Zhang, Y.; Duan, Y.; Wang, T.; *Phys. Chem. Chem. Phys.* **2014**, *16*, 26261. [Crossref]
5. Pan, W.; Zhang, Q.; Chen, Y.; *Optoelectron. Adv. Mater., Rapid Commun.* **2010**, *4*, 2118. [Crossref]
6. Shumakovich, G.; Kurova, V.; Vasil'Eva, I.; Pankratovc, D.; Otrokhova, G.; Morozovaa, O.; Yaropolov, A.; *J. Mol. Catal. B: Enzym.* **2012**, *77*, 105. [Crossref]
7. Stejskal, J.; Exnerová, M.; Morávková, Z.; Trchová, M.;

Hromádková, J.; Prokeš, J.; *Polym. Degrad. Stab.* **2012**, *97*, 1026. [Crossref]
8. Mustapa, R.; Mansor, Z. I. A.; Sambasevam, K. P.; *J. Phys. Sci.* **2018**, *29*, 9. [Crossref]
9. Rahaman, M.; Chaki, T. K.; Khastgir, D.; *J. Appl. Polym. Sci.* **2013**, *128*, 161. [Crossref]
10. Chang, Y. H.; Chang, C. C.; Chang, L. Y.; Wang, P. C.; Kanokpaka, P.; Yeh, M. H.; *Nano Energy* **2023**, *112*, 108505. [Crossref]
11. Ramaprasad, A. T.; Rao, V.; *Sens. Actuators, B* **2010**, *148*, 117. [Crossref]
12. Jaaoh, D.; Putson, C.; Muensit, N.; *Polymer* **2015**, *61*, 123. [Crossref]
13. Sathiyanarayanan, S.; Karpakam, V.; Kamaraj, K.; Muthukrishnan, S.; Venkatachari, G.; *Surf. Coat. Technol.* **2010**, *204*, 1426. [Crossref]
14. Bertuoli, P. T.; Baldissera, A. F.; Zattera, A. J.; Ferreira, C. A.; Alemán, C.; Armelin, E.; *Prog. Org. Coat.* **2019**, *128*, 40. [Crossref]
15. Guo, Y.; Qi, Y.; Zhang, C.; Zhang, S.; Zhanget, Z.; *Polymers* **2023**, *15*, 2944. [Crossref]
16. Rajasekharan, V.; Stalin, T.; Viswanathan, S.; Manisankar, P.; *Int. J. Electrochem. Sci.* **2013**, *8*, 11327. [Crossref]
17. Wang, F.; Min, S. X.; *Chin. Chem. Lett.* **2007**, *18*, 1273. [Crossref]
18. Jumat, N. A.; Wai, P. S.; Ching, J. J.; Basirun, W. J.; *Polym. Polym. Compos.* **2017**, *25*, 507. [Crossref]
19. Varela, H.; Torresi, R. M.; Buttry, D. A.; *J. Braz. Chem. Soc.* **2000**, *11*, 32. [Crossref]
20. Huguenin, F.; Torresi, R. M.; *Quim. Nova* **2004**, *27*, 393. [Crossref]
21. Wang, Y.; Liu, A.; Li, T.; Han, Y.; Ma, Y.; Zhang, Q.; Zhang, J.; *J. Electron. Mater.* **2020**, *49*, 3751. [Crossref]
22. Bilal, S.; Begum, B.; Gul, S.; Shah, A. A.; *Synth. Met.* **2018**, *235*, 1. [Crossref]
23. Xu, L. L.; Xu, Y.; Liu, L.; Wang, K.; Patterson, D.; Wang, J.; *J. Membr. Sci.* **2019**, *572*, 442. [Crossref]
24. Araújo, O. A.; de Paoli, M. A.; *Synth. Met.* **2009**, *159*, 1968. [Crossref]
25. Minisy, I. M.; Salahuddin, N. A.; Ayad, M. M.; *Appl. Clay Sci.* **2021**, *203*, 105993. [Crossref]
26. Wang, H.; Wang, W.; Yu, H.; Mao, Q.; Xu, Y.; Li, X.; Wang, Z.; Wang, L.; *Appl. Catal., B* **2022**, *307*, 121172. [Crossref]
27. Khodabandehlo, A.; Noori, A.; Rahmanifar, M. S.; El-Kady, M. F.; Kaner, R. B.; Mousavi, M. F.; *Adv. Funct. Mater.* **2022**, *32*, 2204555. [Crossref]
28. Bednarczyk, K.; Matysiak, W.; Tański, T.; Janeczek, H.; Balcerzak, E. S.; Libera, M.; *Sci. Rep.* **2021**, *11*, 7487. [Crossref]
29. Xia, H.; Wang, Q.; *Chem. Mater.* **2002**, *14*, 2158. [Crossref]
30. Bhadra, S.; Khastgir, D.; Singha, N. K.; Lee, J.; *Prog. Polym. Sci.* **2009**, *34*, 783. [Crossref]
31. Hino, T.; Seida, Y.; Takahashi, T.; Kuramoto, N.; *Polym. Int.* **2006**, *55*, 243. [Crossref]
32. Khairy, M.; Gouda, M. E.; *J. Adv. Res.* **2015**, *6*, 555. [Crossref]
33. Zhang, Y.; Xi, Q.; Chen, J.; Duan, Y.; *J. Cluster Sci.* **2014**, *25*, 1501. [Crossref]
34. Gomes E. C.; Oliveira M. A. S.; *Am. J. Polym. Sci.* **2012**, *2*, 5. [Crossref]
35. Bhadra, J.; Madi, N. K.; Al-Thani, N. J.; Al-Maadeed, M.; *Synth. Met.* **2014**, *191*, 126. [Crossref]
36. Anwer, T.; Ansari, M. O.; Mohammad, F.; *J. Ind. Eng. Chem.* **2013**, *19*, 1653. [Crossref]
37. Morgon, N. H.; *Quim. Nova* **2001**, *24*, 676. [Crossref]
38. Boudreaux, D. S.; Chance, R. R.; Wolf, J. F.; Shacklette, L.; Brédas, J.; Thémans, B.; André, J.; Silbey, R.; *J. Chem. Phys.* **1986**, *85*, 4584. [Crossref]
39. Alghunaim, N. S.; *J. Inorg. Organomet. Polym. Mater.* **2018**, *28*, 2721. [Crossref]
40. Singh, S.; Tripathi, R. K.; Gupta, M. K.; Dzhardimalieva, G.; Uflyand, I.; Yadav, B.; *J. Colloid Interface Sci.* **2021**, *600*, 572. [Crossref]
41. Benafqir, M.; Hsini, A.; Laabd, M.; Laktif, T.; Ait Addi, A.; Albourine, A.; El Alem, N.; *Sep. Purif. Technol.* **2020**, *236*, 116286. [Crossref]
42. Oliveira, G. P.; Barboza, B. H.; Batagin-Neto, A.; *Comput. Theor. Chem.* **2022**, *1207*, 113526. [Crossref]
43. Sharma, D.; Singh, T.; *J. Mol. Liq.* **2019**, *293*, 111528. [Crossref]
44. Shi, H.; Wu, T. R.; Qiao, H. T.; Gao, Z.; Zhou, J.; Wu, D.; Tian, Z.; *J. Phys. Chem. C* **2023**, *127*, 12357. [Crossref]
45. Ergönenç Yavas, Z.; Cevher, D.; Silis, H.; Cirpan, A.; Gülseren, O.; Franchini, C.; *J. Phys. Chem. C* **2023**, *127*, 6813. [Crossref]
46. Jebakumar, A. A.; Premkumar P. S.; Jeyamalar, J. I.; Raj, C. R. S.; *BioGecko* **2023**, *12*, 3989. [Link] accessed in August 2024
47. Stewart, J. J. P.; *MOPAC*, version 2016; Stewart Computational Chemistry, Colorado Springs, CO, USA, 2016.
48. Frisch, M. J.; Trucks, G. W.; Schlegel, H. B.; Scuseria, G. E.; Robb, M. A.; Cheeseman, J. A.; Montgomery Jr., J. A.; Vreven, T.; Kudin, K. N.; Burant, J. C.; Millam, J. M.; Iyengar, S. S.; Tomasi, J.; Barone, V.; Mennucci, B.; Cossi, M.; Scalmani, G.; Rega, N.; Peterson, G. A.; Nakatsuji, H.; Hada, M.; Ehara, M.; Toyota, K.; Fukuda, R.; Hasegawa, J.; Ishida, M.; Nakajima, T.; Honda, Y.; Kitao, O.; Nakai, H.; Klene, M.; Li, X.; Know, J. E.; Hratchian, H. P.; Cross, J. B.; Adamo, C.; Jaramillo, J.; Gomperts, R.; Stratmann, R. E.; Yazyev, O.; Austin, A. J.; Cammi, R.; Pomelli, C.; Ochterski, J. W.; Ayala, P. Y.; Morokuma, K.; Voth, G. A.; Salvador, P.; Dannenberg, J. J.; Zakrzewski, V. G.; Dapprich, S.; Daniels, A. D.; Strain, M. C.; Farkas, O.; Malick, D. K.; Rabuck, A. D.; Raghavachari, K.; Foresman, J. B.; Ortiz, J. V.; Cui, Q.; Baboul, A. G.; Clifford, S.; Cioslowski, J.; Stefanov, B. B.; Liu, G.; Liashenko, A.; Piskorz, P.; Komaromi, I.; Martin, R. L.; Fox, D. J.; Keith, T.; Al-Laham,

M. A.; Peng, C. Y.; Nanayakkara, A.; Challacombe, M.; Gill, P. M. W.; Johnson, B.; Chen, W.; Wong, M. W.; Gonzalez, C.; Pople, J. A.; *Gaussian 03*, revision B.04, Gaussian, Inc., Pittsburgh, PA, USA, 2003.

49. Frisch, M. J.; Trucks, G. W.; Schlegel, H. B.; Scuseria, G. E.; Robb, M. A.; Cheeseman, J. R.; Montgomery Jr., J. A.; Vreven, T.; Kudin, K. N.; Burant, J. C.; Millam, J. M.; Iyengar, S. S.; Tomasi, J.; Barone, V.; Mennucci, B.; Cossi, M.; Scalmani, G.; Rega, N.; Petersson, G. A.; Nakatsuji, H.; Hada, M.; Ehara, M.; Toyota, K.; Fukuda, R.; Hasegawa, J.; Ishida, M.; Nakajima, T.; Honda, Y.; Kitao, O.; Nakai, H.; Klene, M.; Li, X.; Knox, J. E.; Hratchian, H. P.; Cross, J. B.; Bakken, V.; Adamo, C.; Jaramillo, J.; Gomperts, R.; Stratmann, R. E.; Yazyev, O.; Austin, A. J.; Cammi, R.; Pomelli, C.; Ochterski, J. W.; Ayala, P. Y.; Morokuma, K.; Voth, G. A.; Salvador, P.; Dannenberg, J. J.; Zakrzewski, V. G.; Dapprich, S.; Daniels, A. D.; Strain, M. C.; Farkas, O.; Malick, D. K.; Rabuck, A. D.; Raghavachari, K.; Foresman, J. B.; Ortiz, J. V.; Cui, Q.; Baboul, A. G.; Clifford, S.; Cioslowski, J.; Stefanov, B. B.; Liu, G.; Liashenko, A.; Piskorz, P.; Komaromi, I.; Martin, R. L.; Fox, D. J.; Keith, T.; Al-Laham, M. A.; Peng, C. Y.; Nanayakkara, A.; Challacombe, M.; Gill, P. M. W.; Johnson, B.; Chen, W.; Wong, M. W.; Gonzalez, C.; Pople, J. A.; *Gaussian 09*, revision D.01; Gaussian, Inc., Wallingford, CT, USA, 2009.
50. Stojanović, M.; Baranac-Stojanović, M.; *New J. Chem.* **2018**, *42*, 12968. [Crossref]
51. Hussein, R. K.; Elkhair, H. M.; Elzupir, A. O.; Ibnaouf, K.; *J. Ovonic Res.* **2021**, *17*, 23. [Crossref]
52. Massoumi, B.; Aghili, H.; Entezami, A.; *J. Chin. Chem. Soc.* **2009**, *56*, 741. [Crossref]
53. Armes, S. P.; Miller, J. F.; *Synth. Met.* **1988**, *22*, 385. [Crossref]
54. Stejskal, J.; Sapurina, I.; Trchová, M.; *Prog. Polym. Sci.* **2010**, *35*, 1420. [Crossref]
55. Fukui, B. K.; *Angew. Chem., Int. Ed.* **1982**, *21*, 801. [Crossref]
56. Naik J. L.; Reddy, B. V.; Prabavathi, N.; *J. Mol. Struct.* **2015**, *1100*, 43. [Crossref]

*Submitted: April 5, 2024*
*Published online: August 21, 2024*